Recruitment of Neuronal KCNQ2/3 Channels to Membrane Microdomains Depends on Palmitoylation of Alzheimer's Disease-Related Protein BACE1

Gucan Dai

Department of Physiology and Biophysics, University of Washington, Seattle

Correspondence: daig@uw.edu

Key words: KCNQ channels, BACE1, Alzheimer's disease, Palmitoylation

Running title: Recruiting KCNQ2/3 to Lipid Rafts by BACE1

Major and Minor classification: Biological Sciences; Physiology

ABSTRACT (250 words):

β-secretase 1 (β-site amyloid precursor protein (APP)-cleaving enzyme 1, BACE1) plays a crucial role in the amyloidogenesis of Alzheimer's Disease (AD). BACE1 was also discovered to act like an auxiliary subunit to modulate neuronal KCNQ2/3 channels independent of its proteolytic function. BACE1 is palmitoylated at its carboxyl-terminal region, which brings BACE1 to ordered, cholesterol-rich membrane microdomains (rafts). However, the physiological consequences of this specific localization of BACE1 remain elusive. Using spectral Förster Resonance Energy Transfer (FRET), we confirmed BACE1 and KCNQ2/3 channels formed a signaling complex, a phenomenon that was relatively unaffected by the palmitoylation of BACE1. Nevertheless, palmitoylation of BACE1 was required for the recruitment of KCNQ2/3 channels to lipid-raft domains. Mutating the four carboxyl-terminal cysteines (4C/A) of BACE1 abolished the BACE1-dependent increase of FRET between KCNQ2/3 and a lipid raft-specific protein Caveolin1. Furthermore, we used two fluorescent probes, named L10 and S15, to label lipid rafts and non-raft domains of the plasma membrane respectively. Coexpressing BACE1 substantially elevated the FRET between L10 and KCNQ2/3 whereas BACE1-4C/A failed to produce this effect. In contrast, BACE1 had no significant effect on the FRET between S15 probes and KCNQ2/3 channels. In addition, the reduction of BACE1-dependent FRET between raft-targeting L10 probes and KCNQ2/3 channels by applying cholesterol-extracting reagent methyl-β-cyclodextrin (MβCD), raft-disrupting general anesthetics, and pharmacological inhibitors of palmitoylation all supported our hypothesis of the palmitoylation-dependent and raft-specific localization of KCNQ2/3 channels. Collectively, we provide a mechanism underlying how the localization of a neuronal potassium channel is controlled by AD-related protein BACE1.

SIGNIFICANCE STATEMENT (120 words):

Alzheimer's disease (AD) has no effective cure. Animals with knockout of the key related enzyme BACE1 do not generate β-amyloids or develop AD, but rather exhibit altered behaviors and neuronal deficits. A new linkage between BACE1 and neuronal excitability is the interaction between BACE1 and KCNQ channels. KCNQ channels function as a brake for excessive neuronal excitabilities and are modulated by interacting with BACE1. We revealed a mechanism that BACE1 helps to recruit KCNQ channels to membrane microdomains called rafts. This

localization of KCNQ channels is dependent on a specific type of lipidation of BACE1. This mechanism advances our understanding of AD pathophysiology and could potentially provide therapeutic interventions when rescuing the neuronal abnormalities after ablating BACE1 genetically is needed.

INTRODUCTION

Alzheimer's disease (AD), the most prevalent form of dementia, is characterized by high amount of amyloid plaques in the brain of patients (1, 2). β-secretase 1 (BACE1) is one of the major proteases that cleave the amyloid precursor protein (APP), leading to the accumulation of amyloid β (Aβ) fragments (3). A single mutation in APP that compromises the ability of BACE1 to cleave APP can reduce the Aβ generation and slow the progression of AD (4, 5). Therefore, inhibition of BACE1 was proposed as a promising therapeutic strategy to treat AD (6). Indeed, mice with BACE1 gene knockout, BACE1(-/-), do not develop AD but show changes in behavior tests, including spatial memory deficits, and sensorimotor impairments (7, 8). In addition, BACE1(-/-) mice exhibit neuronal deficits, e.g. axonal organization defects in the hippocampus (9), myelination deficits (10) and altered synaptic function and neurotransmitter metabolism (11). Furthermore, the finding that BACE1(-/-) mice exhibited epileptic seizures promoted the research focusing on the direct role of BACE1 in regulating neuronal voltage-gated sodium and potassium ion channels (12, 13).

One candidate in ion channels that are regulated by BACE1 is the KCNQ family of voltage-gated potassium channels (Kv7) that conduct the neuronal M-current (14, 15). The main neuronal subtypes KCNQ2/3 channels are widely expressed in the nervous system (16) and important for transducing sympathetic stimuli, dampening excessive neuronal excitability, reducing excitatory postsynaptic potentials and controlling synchronized neuronal firings (17, 18). KCNQ2/3 channels are abundantly present in the brain, especially in hippocampus and are critical for hippocampal excitability (19-22). In 2015, BACE1 was reported to interact with KCNQ2/3 channels directly to potentiate M-currents in hippocampus (15). Using patch-clamp electrophysiology, immunoprecipitation, proximity-ligation assay, BACE1 was shown to function as an auxiliary subunit of KCNQ2/3 channels, independent of its proteolytic activity (15). Since KCNQ channel genes are well known for their involvement in several types of epilepsy (23, 24), this research seemingly provides a novel linkage between KCNQ2/3 channels and the epileptic phenotypes seen in BACE1(-/-) mice. Not surprisingly, it was also found that AD patients are more susceptible to develop epilepsy (25).

BACE1's enzymatic activity as the protease of APP occurs in membrane lipid rafts (26, 27). Lipid rafts are dynamic membrane microdomains that are assembled by sphingolipids, cholesterols, and proteins (28). Rafts are detergent-resistant membrane fractions, structurally more ordered than non-raft areas, and are signaling hubs for orchestrating many cellular events (29). Lipid raft-localization of BACE1 favors the processing of APP in the amyloidogenic direction, generating Aβ (27). When APPs are outside of the rafts, they are preferred to be cleaved by the non-amyloidogenic α-secretase. Similar to other raft-localizing proteins like tyrosine kinases, G protein α-subunits, and ATP receptors, BACE1 uses palmitoylation of four cysteines at its carboxyl-terminal end for this specific membrane anchoring (30). However, it is not well understood where the non-enzymatic activities of BACE1 happen, especially for regulating KCNQ channels. KCNQ channels do not have known palmitoylation sites, but are

reported to interact with palmitoylated scaffold proteins, e.g. A-kinase anchoring proteins (AKAP79 in human) and ankryrin-G (31-34). Furthermore, previous research suggested that there was spatial overlap in the subcellular localization of BACE1 and KCNQ channels: KCNQ channels are thought to be localized in axons and axonal initial segments (AIS) via ankyrin-G whereas BACE1 are abundant in axons and implicated in the myelination of axons functionally (10, 31, 35).

To understand the regulation of KCNQ2/3 channels by BACE1, we investigated the localization of the BACE1-KCNQ complex in the lipid rafts of cultured cells and provided further evidence supporting the interaction of BACE and KCNQ2/3. We used Förster Resonance Energy Transfer (FRET) to determine the proximity of membrane proteins and measured FRET, in a spectral manner, based on the sensitized emission of FRET acceptor after exciting the FRET donor. Using engineered fluorescent probes, derived from short lipidated sequences of protein kinases Lck and Src, to label lipid rafts and non-raft domains respectively (36, 37), we saw compelling evidence that KCNQ channels are localized to lipid rafts. This specific localization of KCNQ channels is dependent on the palmitoylation of BACE1. The non-enzymatic activity of BACE1, particularly for regulating KCNQ channels also relies on its localization in lipid rafts. We provide a strategy to determine the localization of proteins in specific lipid microdomains, which could be broadly applied to answer similar questions of other membrane proteins.

RESULTS

This article reports the specific localization of neuronal KCNQ2/3 channels in membrane microdomains (lipid rafts), controlled by the complex formation with β-secretase 1 (BACE1).

FRET between KCNQ2/3 and BACE1 was consistent with their close assembly.

BACE1 interacts with KCNQ2/3 channels directly. Since KCNQ channels often assemble with single-transmembrane auxiliary subunits e.g. the KCNE1 for cardiac KCNQ1 channels (17), BACE1, which is also a single-transmembrane protein, functions like a novel auxiliary subunit for KCNQ2/3 channels by analogy (15). The atomic details of the interaction between BACE1 and KCNQ2/3 are largely unknown. Here, we further tested this interaction using FRET between a fluorescent noncanonical-amino acid L-Anap (38, 39) (Fig. S1) incorporated into the carboxyl-terminal end of a mouse BACE1 and yellow fluorescent proteins (YFP) fused to the carboxyl-terminus of both human KCNQ2 and KCNQ3 subunits all expressed in a cell line tsA201 derived from human embryonic kidney cells. KCNQ2 and KCNQ3 subunits formed heteromeric channel complex and were always expressed together throughout this paper.

BACE1 consists of an extracellular (amino-terminal) proteolytic domain, a helical transmembrane domain and a short intracellular (carboxyl-terminal) region (Fig. 1A). Four cysteines, one in the transmembrane domain(C474) and three within the intracellular region (C478, C482, C485) are palmitoylated for the lipid raft-localization of BACE1. Mutating these cysteines for S-palmitoylation was reported to reduce the raft localization of BACE1 but did not completely abolish the processing of APP by BACE1. The DXXLL motif at the carboxyl-terminal end of BACE1 is involved in the endocytosis and retrograde transport of BACE1 to trans-Golgi networks (40, 41). Mutating this motif increases the plasma membrane localization of BACE1 (41). In addition, the transmembrane and carboxyl-terminal region of BACE1 is highly conserved (almost identical) among different species (Fig. 1A).

Amber stop-codon (TAG) suppression strategy (38) was used to incorporate L-Anap at the leucine 500 (L500) position within the DXXLL motif of BACE1 (Fig S1). To express BACE1-L500Anap in tsA201 cells, cells were transiently transfected with the BACE1-L500TAG cDNA and a plasmid pANAP encoding for the orthogonal amber suppressor tRNA/aminoacyl-tRNA synthetase (aaRS) pair for L-Anap and incubated overnight with culture media supplemented with 20 μM membrane-permeable methyl-ester form of L-Anap (42). When the translation machinery arrives at the TAG stop-codon site, the translation continues by including L-Anap, avoiding its termination. This strategy has previously been shown to achieve satisfactory incorporation of L-Anap to exogenously-expressed recombinant membrane proteins (43, 44). In our experiments, cells grown without applying pANAP plasmid (tRNA/aaRS), but with BACE1-L500TAG cDNA transfected and L-Anap in media were used as negative controls for the FRET experiments.

FRET between L-Anap and YFP were determined by measuring the emission spectra of both fluorophores using a spectrometer attached to the microscope. This type of spectrum-based FRET is capable to correct for the bleed-through and the cross-talk due to spectral properties of FRET donors and acceptors (see Methods). The Anap emission spectrum overlaps well with the excitation spectrum of YFP, making them a feasible FRET pair (38, 43). A high FRET indicates a close assembly of two proteins. The cells that expressed BACE1-L500TAG alone were used to generate a L-Anap emission spectrum (cyan spectrum in Fig. 1B) to correct for the bleed-through of the Anap emission in the wavelength range for YFP emission. The cyan spectrum in Fig. 1B was normalized and subtracted from the L-Anap spectra measured when KCNQ2/3-YFP channels were present. In addition, the cells that only expressed KCNQ2/3-YFP channels (no FRET donor) were excited by Anap excitation, generating a spectrum with its amplitude only a small fraction (0.06) of the YFP emission directly excited by YFP excitation. This was used to correct the cross-talk of FRET (Fig. 1C). The calculated apparent FRET efficiencies were also related to the relative expression levels of L-Anap-incorporated BACE1 and KCNQ2/3-YFP. This apparent FRET efficiency is linearly proportional to the absolute FRET efficiency occurring in the system and are correlated positively with the ratio of Anap versus YFP peak fluorescence intensities (Fig. 1B and D). This positive correlation is typical for ensemble FRET with unfixed stoichiometries and could be fitted with a simple Langmuir isotherm (45, 46). In the rest of the paper, we also used the similar spectral FRET for the cyan fluorescent protein (CFP) and YFP pairs (see Methods).

The FRET between BACE1-L500Anap and KCNQ2/3-YFP show similar apparent efficiencies (no statistical difference) comparing the normal condition to the conditions when the four palmitoylated cysteines in BACE1 were mutated to alanines (4C/A) and when cells were incubated with the palmitoylation inhibitor 2-bromopalmitate (47) (0.1 mM 2-BP) (Fig. 1D and E). The negative-control cells without pANAP plasmid transfected showed minimal FRET despite visible Anap fluorescence was present due to the nonspecific entry of L-Anap to cells. Furthermore, another voltage-gated potassium channel KCNH (a zebrafish ELK) (44), that was considered to be structurally similar to KCNQ but have no reported interaction with BACE1, showed negligible FRET (Fig 1D and E). These results, together with previously-published work, suggest that BACE1 and KCNQ2/3 channels form a protein complex, which is relatively independent of the palmitoylation of BACE1.

Proximity between KCNQ2/3 and the raft-protein caveolin1, conferred by BACE1

If KCNQ2/3 forms a complex with BACE1, could their lipid-raft localization be detected experimentally? We used a protein caveolin 1 (CAV1), which is one of the main components of caveoleo and specific to lipid rafts (46, 48, 49), to test this idea. Caveolin1 often dimerizes at its amino-terminal regions and uses the palmitoylation of three cysteines at its carboxyl-terminal side to target to lipid rafts (46, 49). A carboxyl-terminal CFP-tagged caveolin 1 was coexpressed with KCNQ2/3-YFP channels in tsA cells and their FRET was measured in the same spectral manner. Without BACE1, the FRET between caveolin 1-CFP and KCNQ2/3-YFP is low (Fig 2A, E and F). The relationship between the apparent FRET efficiency and the ratio of CFP/YFP was also fitted with the Langmuir isotherm (Fig. 2E). A nonlinear saturating fitting curve in Fig. 2 E suggested clustering of fluorescent molecules whereas a more linear-looking curve indicated a low level of clustering (50). With the coexpression of BACE1, there were a dramatic increase in the apparent FRET intensities, a leftward shift and a more saturating characteristic for the relationship between the FRET and the donor/acceptor ratio. The possible clustering of molecules could be due to the oligomerization of caveolin 1-CFP in the lipid rafts. In contrast, when coexpressed with the BACE1-4C/A construct, the CFP-YFP FRET was diminished substantially. The relationship between FRET and donor/acceptor ratio with BACE1-4C/A resembled to that in the condition without BACE1. In the representative FRET spectrographs in the Fig. 2 A-C, similar ratio of CFP/YFP intensities was presented for a clear comparison of the FRET efficiency. Together, these results suggest that, with the help of BACE1, KCNQ2/3 channels become closer to lipid-raft domains and can FRET more efficiently with raft-specific proteins CAV1. Endogenous BACE1 was reported to be present in human embryonic kidney cells (based on the Human Protein Atlas, proteinatlas.org), but in our overexpression system, endogenous BACE1 or other scaffold proteins may not be abundant enough to bring overexpressed KCNQ2/3 channels to lipid rafts.

Using fluorescent probes that target lipid raft and non-raft domains

To further study the lipid raft-localization of KCNQ2/3 channels, we resorted to two fluorescent probes that can be targeted to ordered and disordered domains at the plasma membrane (Fig. 3A). The L10 probe derives from the first 10 amino acids from the amino terminus of Lck kinase, which contains two palmitoylation sites for localizing to the ordered lipid-raft domain (36, 37). In contrast, the Src kinase-derived S15 probe (first 15 amino acids from the amino-terminus of Src), which has one myristoylation site, targets to the lipid disordered non-raft domains (36, 37).

Validating FRET experiments were first performed between the Caveolin 1-CFP/L10-YFP as well as Caveolin 1-YFP/S15-YFP FRET pairs (Fig 3 B-D). As expected, L10 and Caveolin 1 exhibited much higher FRET than the FRET between S15 and Caveolin 1, indicating the colocalization of L10 and Caveolin 1 in raft microdomains. Consistent with previous research, plotting the relationship between the apparent FRET efficiency versus the ratio (CFP/YFP) also revealed saturating fitted curves, indicating the clustering of fluorescent molecules in a small area. Since the lipid rafts are considered small in size (< 250 nm in diameter), conventional fluorescent microscopy that is hindered by the diffraction limit of light cannot visualize them reliably. Our FRET method provides an alternative to quantitatively measure the colocalization of proteins in small raft areas.

Next, L10 and S15 probes were used to test their colocalizations with KCNQ2/3 channels and how they are regulated by BACE1. L10-CFP probes were coexpressed with KCNQ2/3-YFP channels. We found adding BACE1 significantly elevated the FRET between L10-CFP and KCNQ2/3-YFP whereas BACE1-4C/A was not able to produce an appreciable change in the

FRET (Fig 4 A and C). However, using the same experimental settings, BACE1 did not affect the FRET between S15-CFP and KCNQ2/3-YFP. BACE1-4C/A construct did not affect the S15-CFP/KCNQ2/3-YFP FRET either (Fig 4 B and D). To summarize, overexpressed KCNQ2/3 channels do show higher colocalization with S15 than with L10 (highlighted in Figure S3 B). However, coexpressing BACE1 can significantly increase the localization of KCNQ2/3 channels in lipid rafts due to a direct interaction between KCNQ and BACE1. In the latter case with BACE1, KCNQ2/3 showed higher FRET with L10 than with S15. Mutating the 4 cysteines in BACE1 for palmitoylation can eliminate this effect, corroborating the critical role of palmitoylation for the lipid raft-localization of BACE1 and its partner KCNQ2/3.

Furthermore, several pharmacological manipulations were applied to the cells showing high FRET between L10-CFP and KCNQ2/3-YFP in the presence of wild-type BACE1 (Fig. 4 E and F). We used cholesterol-extracting methyl-β-cyclodextrin (MβCD) in the medium, which could efficiently decrease plasma membrane cholesterol levels and reduce the raft areas. MβCD application decreased the FRET between L10-CFP and KCNQ2/3-YFP considerably, suggesting this FRET is dependent on the raft domains as well as cholesterols that help to maintain the rafts (Fig. 4 E and F). General anesthetics also work by disrupting lipid rafts for their medical use (51). We found one potent general anesthetic chloroform dramatically suppressed the FRET between L10-CFP and KCNQ2/3-YFP, similar to the effect of MβCD. In addition, 2-BP that inhibited palmitoylation abolished the FRET, indicating again that the palmitoylation is required for the BACE1-dependent localization of KCNQ2/3 channels to lipid rafts (Fig 4 E and F).

Similar distribution of PI(4,5)P_2 in both rafts and non-rafts

Lastly, we explored one possibility for the mechanism of the regulation of KCNQ2/3 channel function by BACE1, focusing on membrane phospholipid phosphatidylinositol 4,5-bisphosphate (PI(4,5)P_2). PI(4,5)P_2 is a signaling lipid that is required for KCNQ2/3 channel activation (52-54). A YFP-tagged PI(4,5)P_2 sensor Tubby was used to label PI(4,5)P_2 (54). FRET efficiencies between Tubby-YFP and either L10-CFP or S15-CFP were equally high but indistinguishable in amplitude (Figure S3). In this case, presumably, CFP and YFP were both next to the lipid bilayer and closer to each other in distance, due to the smaller PI(4,5)P_2-binding domain in Tubby in comparison to the large carboxyl-terminal regions of KCNQ2/3. However, the similar FRET for L10 and S15 suggested that PI(4,5)P_2 are similarly present in both lipid rafts and non-raft domains. In other words, PI(4,5)P_2 appears to be uniformly present at the plasma membrane. We may exclude PI(4,5)P_2 as a key factor that determines the change of KCNQ2/3 function by forming the complex with BACE1.

DISSCUSION

Using FRET, the spectroscopic distance ruler, we found KCNQ2/3 channels are in proximity to lipid-raft markers and raft-specific proteins. We propose that neuronal KCNQ2/3 channels are localized to or close to the ordered membrane microdomain lipid rafts. This localization is achieved by the interaction between KCNQ2/3 and BACE1 and is dependent on the S-palmitoylation of 4 cysteines in the BACE1 carboxyl terminus. Without BACE1, KCNQ2/3 channels at the plasma membrane might be distributed more in the disordered non-raft areas at least in our heterologous expression system. Palmitoylation alters the ion channel localization and affect KCNQ channels indirectly via an auxiliary subunit BACE1 in this case. This type of

ion channel regulation by S-palmitoylation is distinct from the direct lipidation and anchoring of ion-channel domains to lipid bilayers, thereby changing its gating, e.g. palmitoylation of the $P2X_7$ ATP receptor prevents its desensitization (55). Furthermore, this indirect regulation is analogous to the inhibition of the cardiac sodium/potassium pump by palmitoylation of the auxiliary phosphoprotein phospholemman (56).

Palmitoylation manifests an important way for localizing cell signaling, from cellular excitability to massive endocytosis (30, 57). For membrane proteins, 16 carbon S-palmitoylation is reversible and controlled by Asp-His-His-Cys acyltransferase (e.g. plasma membrane DHHC5), which is thought to be abundant in ordered lipid microdomains (30, 56). The 2-BP inhibition of KCNQ2/3 localization to rafts suggests that the potassium channel function could also be indirectly affected by acyltransferases and subject to modulation by lipid metabolism. Specifically, it is reasonable to predict that KCNQ channel function could be modulated by cellular signals that are upstream of DHHC, like generation of reactive oxygen species (ROS) (58), opening of mitochondrial permeability transition pores (PTPs), coenzyme A (CoA) release etc (57, 59). Furthermore, in native neuronal environments, KCNQ2/3 channels are localized to axons by interacting with palmitoylated ankyrin G, which itself could possibly recruit KCNQ2/3 channels to lipid rafts (31, 33). This ankyrin-G interaction could also facilitate the interaction of KCNQ2/3 with BACE1. The synergistic effect of the palmitoylations of KCNQ2/3-associated proteins including ankyrin G, BACE1 and AKAP79 remains elusive.

This research provides a new function for the raft-localization of BACE1, independent of the proteolytic or amyloidogenic features of BACE1. Previous research has shown that abolishing the raft-localization of BACE1 reduces the amyloid production and mitigates memory deficits in transgenic mouse models of Alzheimer's disease (60). Conversely, targeting BACE1 to lipid rafts by glycosylphosphatidylinositol (GPI)-anchor elevates the β-site processing of the amyloid precursor protein (26). Despite these findings, this role of the raft-localization of BACE1 for APP processing is still debatable; other research suggested that the Aβ production was still present even in the absence of the palmitoylation-dependent targeting of BACE1 to lipid rafts (61). Here, the new function of the raft-localization of BACE1 for the KCNQ2/3 channel function could play a role in reducing neuronal electrical excitability (22), modulating afterhyperpolarization potentials (AHP) (62, 63), and maintaining the proper propagation of nerve spikes (20). It remains to be determined that if the KCNQ2/3 channel activity affects the ability of BACE1 to cleave APP and to generate amyloid-β peptides reciprocally.

The disruption of lipid rafts underlies the mechanism for the medical effect of general anesthetics (51). Lipid-soluble general anesthetics change the lipid organization of sphingomyelin- and cholesterol-rich rafts, displace phospholipase D (PLD) from rafts to non-raft areas, which in turn generates phosphatidic acids (PA) that activate K_{2P} (TREK) ion channels (51). We found that applying chloroform was able to decrease the FRET between KCNQ2/3 with the raft-marker L10, indicating that general anesthetics similarly displaces KCNQ2/3 to non-raft areas and could possibly alter the activity of KCNQ2/3 channels. Since we do not think $PI(4,5)P_2$ is present in both rafts and non-rafts, and relatively-uniformly distributed at the plasma membrane, other molecular components intrinsic to the lipid rafts might contribute more to the effect of BACE1 on KCNQ2/3. Consistently, hydrolysis of $PI(4,5)P_2$ did not seem to affect the electrophysiological changes of KCNQ2/3 caused by BACE1 coexpression (15). Future research will be needed to further understand the detailed molecular mechanism underlying the regulation of KCNQ2/3 channels by BACE1.

MATERIALS AND METHODS

Cell Culture, Molecular Biology and Reagents

The tsA-201 cells were cultured, maintained and transfected as previously reported (54). Point mutations were made using Quickchange II XL Site-Directed Mutagenesis kit (Agilent technologies, Santa Clara, CA). The sequences of the DNA constructs were confirmed by fluorescence-based DNA sequencing (Genewiz LLC, Seattle, WA). The mBACE1 construct was obtained from Addgene (Cambridge, MA). L-Anap (AsisChem, Waltham, MA) was made as a 10 mM stock, stored at −20°C and diluted by 500-fold into culture medium. The fluorescent L10 and S15 constructs were made in the lab of Dr. Byung-Chang Suh at Daegu Gyeongbuk Institute of Science and Technology (South Korea) (first used for a unpublished work authored by Jongyun Myeong, Cheon-Gyu Park, Byung-Chang Suh, and Bertil Hille; 09/01/2020). The Caveolin 1 construct was from Suzanne F. Scarlata (Worcester Polytechnic Institute, MA). The pANAP plasmid (Addgene, Cambridge, MA) contained the orthogonal tRNA/aminoacyl-tRNA synthetase specific to L-Anap. 2-bromopalmitate (2-BP) was delivered with fatty acid-free bovine serum albumin (Sigma-Aldrich, A6003) at a stock concentration 1 mM albumin with 5 mM 2-BP, which was diluted by 50-fold into the culture medium generating a final concentration of 0.1 mM 2-BP.

Quantification of FRET and Spectroscopic Analysis

A Nikon Eclipse TE2000-E inverted microscope with a 60X, 1.2 NA water immersion objective was used for fluorescence measurements. Epifluorescence recording was performed with wide-field excitation using a Lambda LS Xenon Arc lamp (Sutter Instruments). For spectral measurements, images were collected by a spectrograph (Model: 2150i, 300 g/mm grating, blaze = 500 nm; Acton research, Acton, MA) mounted between the output port of the microscope and the Evolve 512 EMCCD camera as previously reported (43). A filter cube containing a 376 (centered)/30 (width) nm excitation filter was used for L-Anap. CFP was excited with a filter cube containing a 425/40 nm excitation filter while YFP was excited with a filter cube containing a 490/10 nm excitation filter. A long-pass filter was used for emission measurements of light wavelength > 424 nm (Fig. S2A). Spectral images were collected with exposure times ranging from 200 to 500 ms depending on the fluorescence intensity of the individual cell using an Evolve 512 EMCCD camera (Photometrics, Tucson, AZ) and MetaMorph software (Molecular Devices, Sunnyvale, CA). The exposure time maintained the same for recording donor emission and acceptor emission spectra of the same FRET experiment. The background fluorescence in spectrum was subtracted using areas outside of the cell of interest. All the microscopic experiments were done at room temperature.

FRET donor-only (Anap or CFP) constructs were used to obtain the averaged donor emission spectrum called F(donor) excited by donor excitation wavelength. Furthermore, we normalized the F(donor) to the peak intensity of the $F_{CFP/YFP}{}^{CFP}$ or $F_{Anap/YFP}{}^{Anap}$ spectrum, which is the emission spectrum upon the excitation using donor excitation wavelength when both donors and acceptors are present. The normalized F(donor) was then subtracted from either $F_{CFP/YFP}{}^{CFP}$ or $F_{Anap/YFP}{}^{Anap}$ spectrum in each case, generating spectrum F_{FRET} (for correcting the bleed-through of FRET and in red for all figures). Ratio A was calculated as Ratio A = $F_{FRET} / F_{Anap/YFP}{}^{YFP}$ for the Anap/YFP pair or Ratio A = $F_{FRET} / F_{CFP/YFP}{}^{YFP}$ for the CFP/YFP pair. The denominator of the Ratio A is the spectrum generated by using the excitation light at the YFP excitation wavelength. In addition, two emission spectra were collected from cells that were only transfected with YFP-

containing constructs (in the absence of FRET donors): F_{YFP}^{CFP} or F_{YFP}^{Anap}, the emission spectrum using donor (CFP or Anap) excitation and F_{YFP}^{YFP}, the emission spectrum using acceptor (YFP) excitation. Ratio A0 was calculated using Ratio A0 = F_{YFP}^{Anap}/ F_{YFP}^{YFP} for Anap/YFP FRET pair or Ratio A0 = F_{YFP}^{CFP}/ F_{YFP}^{YFP} for CFP/YFP FRET pair. Ratio A0 corrects for the cross-talk of FRET, which is the fraction of the direct excitation of FRET acceptors by donor-excitation light. Absolute FRET efficiency is linearly proportional to the difference between Ratio A and Ratio A0, hence we call that apparent FRET efficiency = Ratio A – Ratio A0 (45, 64). Ratio A – RatioA0 > 0 indicates a detectable FRET signal.

The relationship between the apparent FRET efficiency (E) and the ratio (R) of the FRET donor to acceptor peak intensity was fitted with a Langmuir isotherm (46): $E = E_{max} * (R / R + K)$, where E_{max} is the maximum apparent FRET efficiency, K is analogous to a dissociation constant for ligand binding and provides an estimate of the degree of clustering at a given concentration of FRET donor relative to the receptor (50). When R << K, E is approximately linear to the FRET-donor surface density. When R >> K, E is mostly saturated and one acceptor is already clustered with at least one donor.

Statistics

The results are presented as mean ± SEM. Statistical significance was determined using the two-tailed Student's t test, *p <0.05.

ACKNOWLEDGMENTS AND FUNDING SOURCES

I thank Drs. Bertil Hille and William N. Zagotta for support; Dr. Donald W. Hilgemann (University of Texas Southwestern) for helpful advice; Drs. Duk-Su Koh, Jongyun Myeong, Seung-Ryoung Jung for discussions. This work was supported by grants from the National Institutes of Health of the United States of America: R37NS08174 and R01EY010329, and by the Wayne E. Crill Endowed Professorship to B.H..

FIGURE LEGENDS:

Figure 1. FRET between L-Anap incorporated in BACE1 and YFP-tagged KCNQ2/3 channels

(A) Sequence alignment of mouse, rat, and human BACE1 proteins highlighting the four cysteines for palmitoylation and the leucine 500 site (*). The transmembrane region is in green. **(B)** Representative emission spectra for the FRET between BACE1-L500Anap and KCNQ2/3-YFP. The cyan and green spectra are generated by the Anap excitation wavelength; the yellow spectrum by YFP excitation; the red spectrum is the subtraction of the cyan spectrum from the green spectrum. **(C)** Representative emission spectrum of KCNQ2/3-YFP-only cells using direct YFP excitation versus the spectrum (smaller amplitude) from the same sample by the excitation for Anap. **(D)** Relationship between the apparent FRET efficiency (Ratio A- Ratio A0) and the ratio of peak intensities of Anap versus YFP. **(E)** Summary of the apparent efficiencies for the FRET (including all the ratio of Anap/YFP measured) between KCNQ2/3 and BACE1 with or without pANAP, BACE1-4C/A, in the presence of 0.1 mM 2-BP as well as FRET between KCNH channel and BACE1; data are shown as mean ± SEM, *p <0.05.

Figure 2. FRET between Caveolin 1-CFP and KCNQ2/3-YFP channels

(A-C) Representative emission spectra for the FRET between Caveolin 1-CFP and KCNQ2/3-YFP. The cyan and green spectra are generated by illumination of the CFP excitation wavelength; the yellow spectrum by YFP excitation; the red spectrum is the subtraction of the cyan spectrum from the green spectrum. **(D)** Representative emission spectrum of KCNQ2/3-YFP alone cells using direct YFP excitation versus the spectrum (smaller amplitude) from the same sample by the excitation for CFP. **(E)** Relationship between the apparent FRET efficiency (Ratio A- Ratio A0) and the ratio of peak intensities of CFP versus YFP for the FRET between KCNQ2/3 and Caveolin in the conditions with or without BACE1 or with BACE1-4C/A. **(F)** Summary of the apparent FRET efficiencies for the same conditions in panel E; data are shown as mean ± SEM, *p <0.05.

Figure 3. Fluorescent probes that target to lipid rafts and non-rafts.

(A) Schematic illustration of L10, S15 as well as Caveolin 1. **(B)** Representative emission spectra for the FRET between Caveolin 1-CFP and L10-YFP. **(C)** Representative emission spectra for the FRET between Caveolin 1-CFP and S15-YFP. **(D)** Relationship between the apparent FRET efficiency and the ratio of peak intensities of CFP versus YFP for the FRET pairs shown in panel B and C.

Figure 4. Using L10, S15 to probe the localization of KCNQ2/3 channels.

Relationship between the apparent FRET efficiency and the ratio (CFP/YFP) for the FRET between the L10-CFP **(A)** or S15-CFP **(B)** and the KCNQ2/3-YFP in the conditions with or without BACE1 or with BACE1-4C/A. **(C)** and **(D)** Summary of the apparent efficiencies for the same conditions in panel A and panel B, respectively **(E)** Relationship between the apparent FRET efficiency and the ratio (CFP/YFP) for the FRET between the L10-CFP and KCNQ2/3-YFP after treating cells with acutely-applied 5 mM MβCD, 1 mM chloroform and 0.1 mM 2-BP. The no treatment control condition, which is the same fitted curve as in the red curve in panel A is shown for clarity. **(F)** Summary of the apparent FRET efficiencies for the same conditions in panel E; data are shown as mean ± SEM, *p <0.05. **(G)** Cartoon illustration summarizing the probing of the localization of KCNQ2/3 channels using L10 and S15 marker.

Figure S1. Schematic illustration of L-Anap incorporation to BACE1

(A) Structure of L-Anap and the Amber stop-codon suppression strategy for incorporating L-Anap**. (B)** Cartoon showing the FRET between BACE1-L500Anap and KCNQ2/3-YFP.

Figure S2. Procedure of performing spectral measurements of cultured cells

(A) Calibration of spectral measurements using different emission filters with Tungsten light illumination. **(B)** Flow-chart illustration of an example of measuring spectral FRET using CFP-tagged and YFP-tagged constructs transfected to tsA cells.

Figure S3. FRET between Tubby-YFP and L10-CFP or S15-CFP.

(A) Representative emission spectra for the FRET between L10-CFP and Tubby-YFP, which labels $PI(4,5)P_2$. **(B)** Relationship between the apparent FRET efficiency and the ratio (CFP/YFP) for the FRET between the L10-CFP or S15-CFP with the Tubby-YFP. The same fitted curves shown in Figure 4 A and B for the FRET between L10-CFP or S15-CFP with the KCNQ2/3-YFP are included for comparison of FRET intensity.

REFERENCES

1. Perl DP (2010) Neuropathology of Alzheimer's disease. *Mt Sinai J Med* 77(1):32-42.
2. Weller J & Budson A (2018) Current understanding of Alzheimer's disease diagnosis and treatment. *F1000Res* 7.
3. Vassar R*, et al.* (2014) Function, therapeutic potential and cell biology of BACE proteases: current status and future prospects. *J Neurochem* 130(1):4-28.
4. Jonsson T*, et al.* (2012) A mutation in APP protects against Alzheimer's disease and age-related cognitive decline. *Nature* 488(7409):96-99.
5. Di Fede G*, et al.* (2009) A recessive mutation in the APP gene with dominant-negative effect on amyloidogenesis. *Science* 323(5920):1473-1477.
6. Vassar R & Kandalepas PC (2011) The β-secretase enzyme BACE1 as a therapeutic target for Alzheimer's disease. *Alzheimers Res Ther* 3(3):20.
7. Cole SL & Vassar R (2007) The Alzheimer's disease β-secretase enzyme, BACE1. *Mol Neurodegener* 2:22.
8. Kobayashi D*, et al.* (2008) BACE1 gene deletion: impact on behavioral function in a model of Alzheimer's disease. *Neurobiol Aging* 29(6):861-873.
9. Ou-Yang MH*, et al.* (2018) Axonal organization defects in the hippocampus of adult conditional BACE1 knockout mice. *Sci Transl Med* 10(459).
10. Hu X*, et al.* (2006) BACE1 modulates myelination in the central and peripheral nervous system. *Nat Neurosci* 9(12):1520-1525.
11. Lombardo S*, et al.* (2019) BACE1 partial deletion induces synaptic plasticity deficit in adult mice. *Sci Rep* 9(1):19877.
12. Lehnert S*, et al.* (2016) Ion channel regulation by β-secretase BACE1-enzymatic and non-enzymatic effects beyond Alzheimer's disease. *Channels (Austin)* 10(5):365-378.
13. Kim DY*, et al.* (2007) BACE1 regulates voltage-gated sodium channels and neuronal activity. *Nat Cell Biol* 9(7):755-764.
14. Brown DA & Adams PR (1980) Muscarinic suppression of a novel voltage-sensitive K^+ current in a vertebrate neurone. *Nature* 283(5748):673-676.
15. Hessler S*, et al.* (2015) β-Secretase BACE1 regulates hippocampal and reconstituted M-currents in a β-subunit-like fashion. *J Neurosci* 35(8):3298-3311.
16. Wang HS*, et al.* (1998) KCNQ2 and KCNQ3 potassium channel subunits: molecular correlates of the M-channel. *Science* 282(5395):1890-1893.
17. Abbott GW (2020) KCNQs: Ligand- and Voltage-Gated Potassium Channels. *Front Physiol* 11:583.
18. Hernandez CC, Zaika O, Tolstykh GP, & Shapiro MS (2008) Regulation of neural KCNQ channels: signalling pathways, structural motifs and functional implications. *J Physiol* 586(7):1811-1821.
19. Shah M, Mistry M, Marsh SJ, Brown DA, & Delmas P (2002) Molecular correlates of the M-current in cultured rat hippocampal neurons. *J Physiol* 544(Pt 1):29-37.
20. Yue C & Yaari Y (2004) KCNQ/M channels control spike afterdepolarization and burst generation in hippocampal neurons. *J Neurosci* 24(19):4614-4624.
21. Klinger F, Gould G, Boehm S, & Shapiro MS (2011) Distribution of M-channel subunits KCNQ2 and KCNQ3 in rat hippocampus. *Neuroimage* 58(3):761-769.
22. Carver CM, Hastings SD, Cook ME, & Shapiro MS (2020) Functional responses of the hippocampus to hyperexcitability depend on directed, neuron-specific KCNQ2 K^+ channel plasticity. *Hippocampus* 30(5):435-455.
23. Biervert C*, et al.* (1998) A potassium channel mutation in neonatal human epilepsy. *Science* 279(5349):403-406.

24. Singh NA*, et al.* (1998) A novel potassium channel gene, KCNQ2, is mutated in an inherited epilepsy of newborns. *Nat Genet* 18(1):25-29.
25. Vossel KA, Tartaglia MC, Nygaard HB, Zeman AZ, & Miller BL (2017) Epileptic activity in Alzheimer's disease: causes and clinical relevance. *Lancet Neurol* 16(4):311-322.
26. Cordy JM, Hussain I, Dingwall C, Hooper NM, & Turner AJ (2003) Exclusively targeting β-secretase to lipid rafts by GPI-anchor addition up-regulates β-site processing of the amyloid precursor protein. *Proc Natl Acad Sci U S A* 100(20):11735-11740.
27. Ehehalt R, Keller P, Haass C, Thiele C, & Simons K (2003) Amyloidogenic processing of the Alzheimer β-amyloid precursor protein depends on lipid rafts. *J Cell Biol* 160(1):113-123.
28. Simons K & Ikonen E (1997) Functional rafts in cell membranes. *Nature* 387(6633):569-572.
29. Lingwood D & Simons K (2010) Lipid rafts as a membrane-organizing principle. *Science* 327(5961):46-50.
30. Linder ME & Deschenes RJ (2007) Palmitoylation: policing protein stability and traffic. *Nat Rev Mol Cell Biol* 8(1):74-84.
31. Chung HJ, Jan YN, & Jan LY (2006) Polarized axonal surface expression of neuronal KCNQ channels is mediated by multiple signals in the KCNQ2 and KCNQ3 C-terminal domains. *Proc Natl Acad Sci U S A* 103(23):8870-8875.
32. Zhang J & Shapiro MS (2016) Mechanisms and dynamics of AKAP79/150-orchestrated multi-protein signalling complexes in brain and peripheral nerve. *J Physiol* 594(1):31-37.
33. He M, Jenkins P, & Bennett V (2012) Cysteine 70 of ankyrin-G is S-palmitoylated and is required for function of ankyrin-G in membrane domain assembly. *J Biol Chem* 287(52):43995-44005.
34. Keith DJ*, et al.* (2012) Palmitoylation of A-kinase anchoring protein 79/150 regulates dendritic endosomal targeting and synaptic plasticity mechanisms. *J Neurosci* 32(21):7119-7136.
35. Buggia-Prevot V*, et al.* (2014) Axonal BACE1 dynamics and targeting in hippocampal neurons: a role for Rab11 GTPase. *Mol Neurodegener* 9:1.
36. Rodgers W (2002) Making membranes green: construction and characterization of GFP-fusion proteins targeted to discrete plasma membrane domains. *Biotechniques* 32(5):1044-1046, 1048, 1050-1041.
37. Chichili GR & Rodgers W (2007) Clustering of membrane raft proteins by the actin cytoskeleton. *J Biol Chem* 282(50):36682-36691.
38. Chatterjee A, Guo J, Lee HS, & Schultz PG (2013) A genetically encoded fluorescent probe in mammalian cells. *J Am Chem Soc* 135(34):12540-12543.
39. Kalstrup T & Blunck R (2013) Dynamics of internal pore opening in K_v channels probed by a fluorescent unnatural amino acid. *Proc Natl Acad Sci U S A* 110(20):8272-8277.
40. Toh WH, Chia PZC, Hossain MI, & Gleeson PA (2018) GGA1 regulates signal-dependent sorting of BACE1 to recycling endosomes, which moderates Aβ production. *Mol Biol Cell* 29(2):191-208.
41. Pastorino L, Ikin AF, Nairn AC, Pursnani A, & Buxbaum JD (2002) The carboxyl-terminus of BACE contains a sorting signal that regulates BACE trafficking but not the formation of total Aβ. *Mol Cell Neurosci* 19(2):175-185.
42. Gordon SE, Munari M, & Zagotta WN (2018) Visualizing conformational dynamics of proteins in solution and at the cell membrane. *Elife* 7.
43. Dai G, Aman TK, DiMaio F, & Zagotta WN (2019) The HCN channel voltage sensor undergoes a large downward motion during hyperpolarization. *Nat Struct Mol Biol*.
44. Dai G & Zagotta WN (2017) Molecular mechanism of voltage-dependent potentiation of KCNH potassium channels. *Elife* 6.
45. Takanishi CL, Bykova EA, Cheng W, & Zheng J (2006) GFP-based FRET analysis in live cells. *Brain Res* 1091(1):132-139.

46. Zacharias DA, Violin JD, Newton AC, & Tsien RY (2002) Partitioning of lipid-modified monomeric GFPs into membrane microdomains of live cells. *Science* 296(5569):913-916.
47. Davda D*, et al.* (2013) Profiling targets of the irreversible palmitoylation inhibitor 2-bromopalmitate. *ACS Chem Biol* 8(9):1912-1917.
48. Li S, Song KS, & Lisanti MP (1996) Expression and characterization of recombinant caveolin. Purification by polyhistidine tagging and cholesterol-dependent incorporation into defined lipid membranes. *J Biol Chem* 271(1):568-573.
49. Williams TM & Lisanti MP (2004) The caveolin proteins. *Genome Biol* 5(3):214.
50. Kenworthy AK & Edidin M (1998) Distribution of a glycosylphosphatidylinositol-anchored protein at the apical surface of MDCK cells examined at a resolution of <100 Å using imaging fluorescence resonance energy transfer. *J Cell Biol* 142(1):69-84.
51. Pavel MA, Petersen EN, Wang H, Lerner RA, & Hansen SB (2020) Studies on the mechanism of general anesthesia. *Proc Natl Acad Sci U S A* 117(24):13757-13766.
52. Suh BC & Hille B (2008) PIP_2 is a necessary cofactor for ion channel function: how and why? *Annu Rev Biophys* 37:175-195.
53. Suh BC & Hille B (2002) Recovery from muscarinic modulation of M current channels requires phosphatidylinositol 4,5-bisphosphate synthesis. *Neuron* 35(3):507-520.
54. Dai G, Yu H, Kruse M, Traynor-Kaplan A, & Hille B (2016) Osmoregulatory inositol transporter SMIT1 modulates electrical activity by adjusting $PI(4,5)P_2$ levels. *Proc Natl Acad Sci U S A* 113(23):E3290-3299.
55. McCarthy AE, Yoshioka C, & Mansoor SE (2019) Full-Length $P2X_7$ Structures Reveal How Palmitoylation Prevents Channel Desensitization. *Cell* 179(3):659-670 e613.
56. Howie J*, et al.* (2014) Substrate recognition by the cell surface palmitoyl transferase DHHC5. *Proc Natl Acad Sci U S A* 111(49):17534-17539.
57. Hilgemann DW*, et al.* (2018) Lipid signaling to membrane proteins: From second messengers to membrane domains and adapter-free endocytosis. *J Gen Physiol* 150(2):211-224.
58. Gamper N*, et al.* (2006) Oxidative modification of M-type K^+ channels as a mechanism of cytoprotective neuronal silencing. *EMBO J* 25(20):4996-5004.
59. Lin MJ*, et al.* (2013) Massive palmitoylation-dependent endocytosis during reoxygenation of anoxic cardiac muscle. *Elife* 2:e01295.
60. Andrew RJ*, et al.* (2017) Lack of BACE1 S-palmitoylation reduces amyloid burden and mitigates memory deficits in transgenic mouse models of Alzheimer's disease. *Proc Natl Acad Sci U S A* 114(45):E9665-E9674.
61. Vetrivel KS*, et al.* (2009) Alzheimer disease Aβ production in the absence of S-palmitoylation-dependent targeting of BACE1 to lipid rafts. *J Biol Chem* 284(6):3793-3803.
62. Gu N, Vervaeke K, Hu H, & Storm JF (2005) Kv7/KCNQ/M and HCN/h, but not $K_{Ca}2$/SK channels, contribute to the somatic medium after-hyperpolarization and excitability control in CA1 hippocampal pyramidal cells. *J Physiol* 566(Pt 3):689-715.
63. Tzingounis AV & Nicoll RA (2008) Contribution of KCNQ2 and KCNQ3 to the medium and slow afterhyperpolarization currents. *Proc Natl Acad Sci U S A* 105(50):19974-19979.
64. Erickson MG, Alseikhan BA, Peterson BZ, & Yue DT (2001) Preassociation of calmodulin with voltage-gated Ca^{2+} channels revealed by FRET in single living cells. *Neuron* 31(6):973-985.

Figure 1

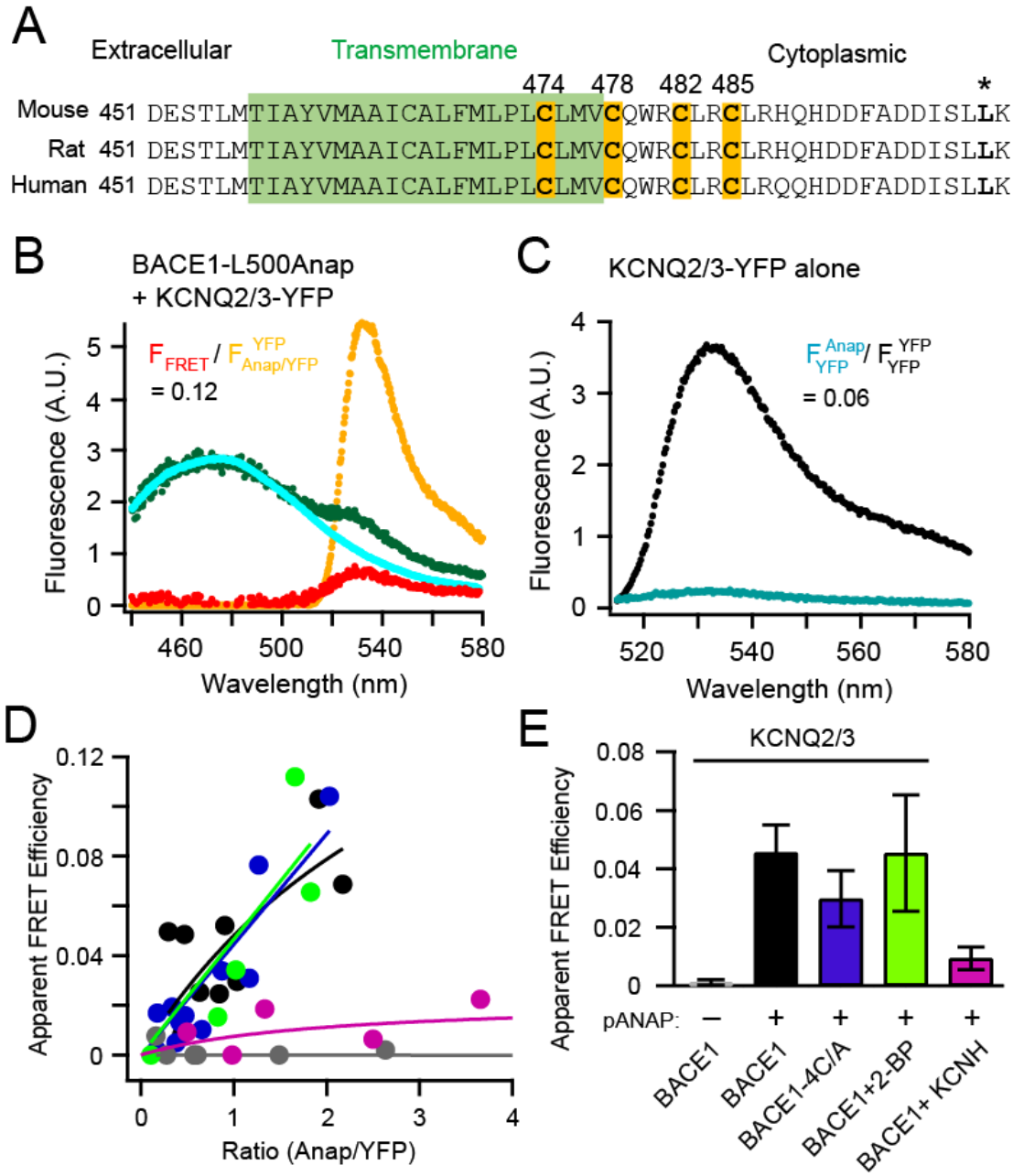
A
Extracellular
Transmembrane
Cytoplasmic
474 478 482 485
*
Mouse 451 DESTLMTIAYVMAAICALFMLPLCLMVCQWRCLRCLRHQHDDFADDISLLK
Rat 451 DESTLMTIAYVMAAICALFMLPLCLMVCQWRCLRCLRHQHDDFADDISLLK
Human 451 DESTLMTIAYVMAAICALFMLPLCLMVCQWRCLRCLRQQHDDFADDISLLK
B
BACE1-L500Anap
+ KCNQ2/3-YFP
F FRET / F YFP Anap/YFP
= 0.12
Fluorescence (A.U.)
Wavelength (nm)
C
KCNQ2/3-YFP alone
F Anap YFP / F YFP YFP
= 0.06
Fluorescence (A.U.)
Wavelength (nm)
D
Apparent FRET Efficiency
Ratio (Anap/YFP)
E
KCNQ2/3
Apparent FRET Efficiency
pANAP: – + + + +
BACE1
BACE1
BACE1-4C/A
BACE1+2-BP
BACE1+ KCNH

Figure 2

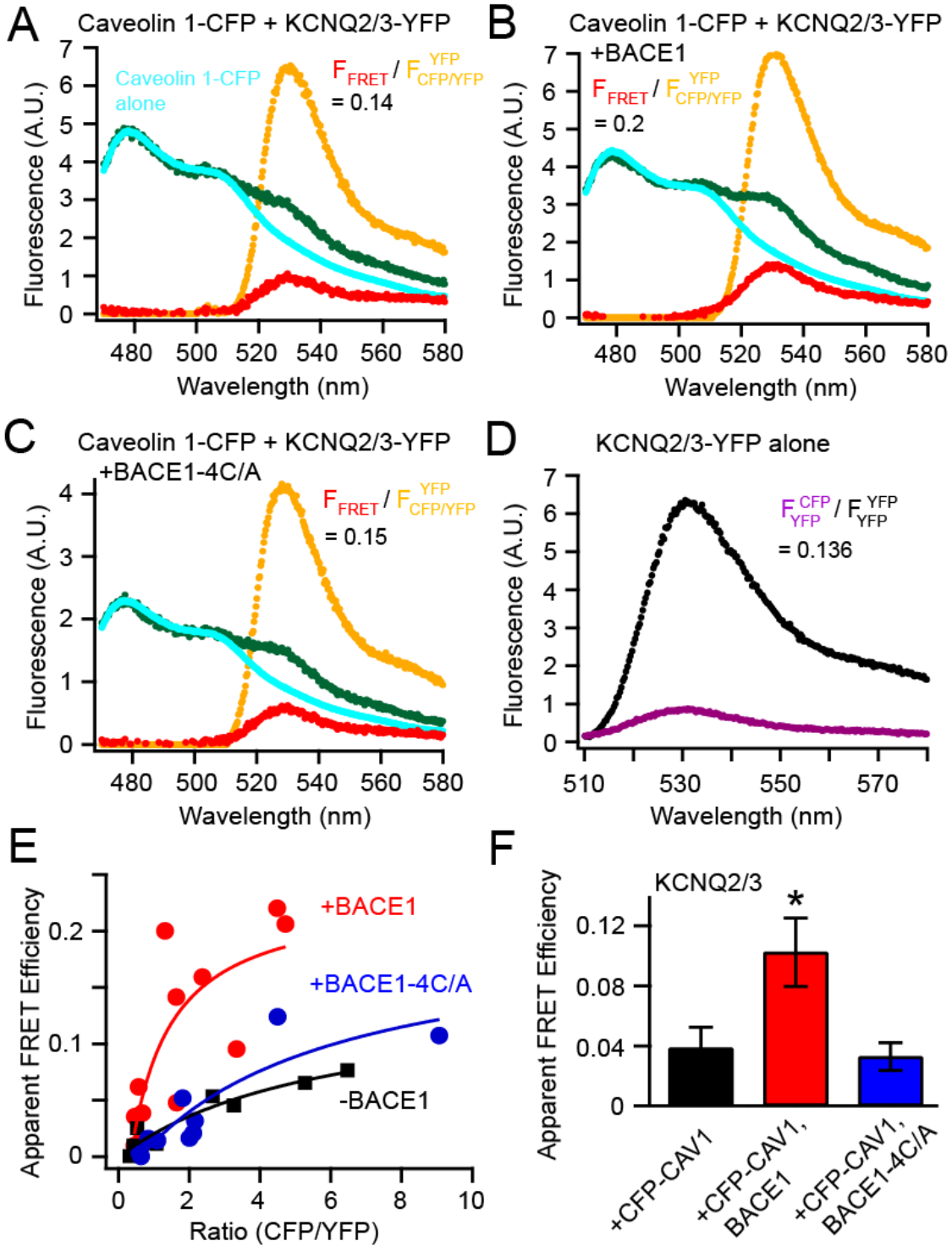
A
Caveolin 1-CFP + KCNQ2/3-YFP
Caveolin 1-CFP alone
$F_{FRET} / F^{YFP}_{CFP/YFP}$ = 0.14
Fluorescence (A.U.)
Wavelength (nm)
B
Caveolin 1-CFP + KCNQ2/3-YFP +BACE1
$F_{FRET} / F^{YFP}_{CFP/YFP}$ = 0.2
C
Caveolin 1-CFP + KCNQ2/3-YFP +BACE1-4C/A
$F_{FRET} / F^{YFP}_{CFP/YFP}$ = 0.15
D
KCNQ2/3-YFP alone
$F^{CFP}_{YFP} / F^{YFP}_{YFP}$ = 0.136
E
Apparent FRET Efficiency
Ratio (CFP/YFP)
+BACE1
+BACE1-4C/A
-BACE1
F
KCNQ2/3
*
+CFP-CAV1
+CFP-CAV1, BACE1
+CFP-CAV1, BACE1-4C/A

Figure 3

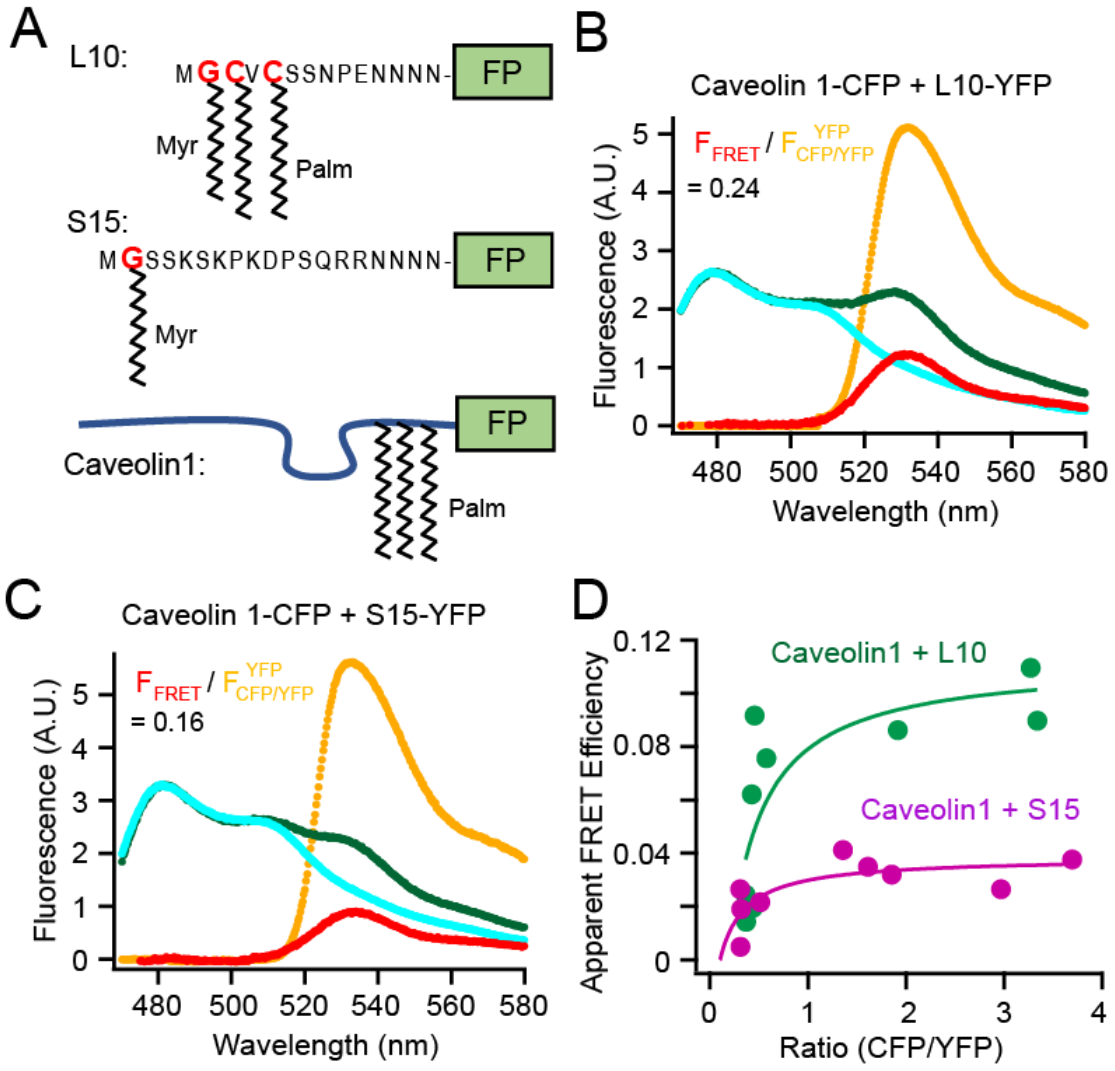
A
L10:
MGCVCSSNPENNNN-
FP
Myr
Palm
S15:
MGSSKSKPKDPSQRRNNNN-
FP
Myr
FP
Caveolin1:
Palm
B
Caveolin 1-CFP + L10-YFP
F FRET / F YFP CFP/YFP
= 0.24
Fluorescence (A.U.)
Wavelength (nm)
C
Caveolin 1-CFP + S15-YFP
F FRET / F YFP CFP/YFP
= 0.16
Fluorescence (A.U.)
Wavelength (nm)
D
Caveolin1 + L10
Caveolin1 + S15
Apparent FRET Efficiency
Ratio (CFP/YFP)

Figure 4

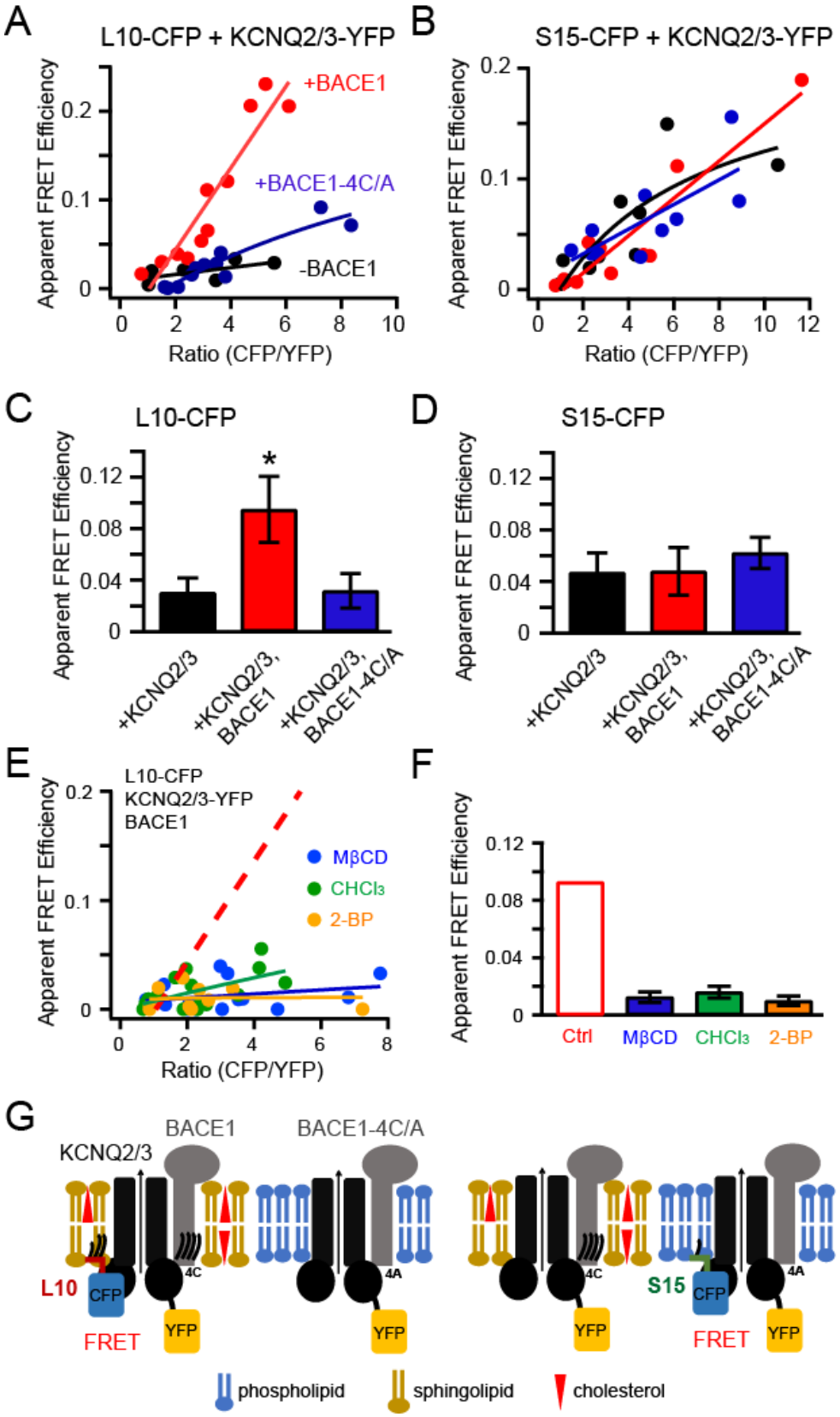
A
L10-CFP + KCNQ2/3-YFP
+BACE1
+BACE1-4C/A
-BACE1
Apparent FRET Efficiency
Ratio (CFP/YFP)
B
S15-CFP + KCNQ2/3-YFP
Apparent FRET Efficiency
Ratio (CFP/YFP)
C
L10-CFP
Apparent FRET Efficiency
+KCNQ2/3
+KCNQ2/3, BACE1
+KCNQ2/3, BACE1-4C/A
D
S15-CFP
Apparent FRET Efficiency
+KCNQ2/3
+KCNQ2/3, BACE1
+KCNQ2/3, BACE1-4C/A
E
L10-CFP
KCNQ2/3-YFP
BACE1
MβCD
CHCl3
2-BP
Apparent FRET Efficiency
Ratio (CFP/YFP)
F
Apparent FRET Efficiency
Ctrl
MβCD
CHCl3
2-BP
G
KCNQ2/3
BACE1
BACE1-4C/A
L10
CFP
YFP
FRET
4C
4A
S15
phospholipid
sphingolipid
cholesterol

Figure S1

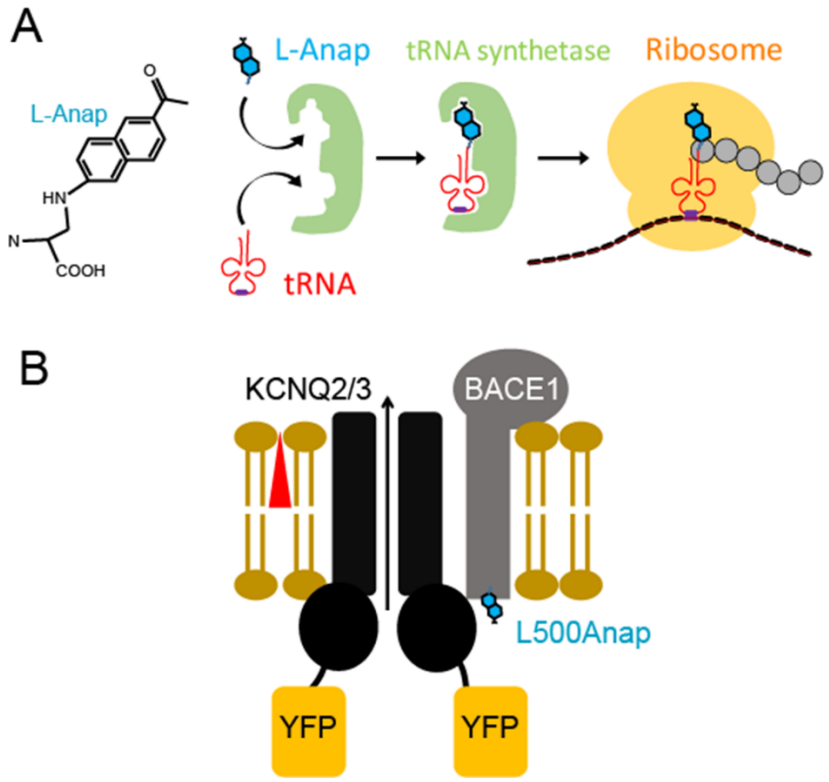
A
L-Anap
O
HN
N
COOH
L-Anap
tRNA synthetase
Ribosome
tRNA
B
KCNQ2/3
BACE1
L500Anap
YFP
YFP

Figure S2

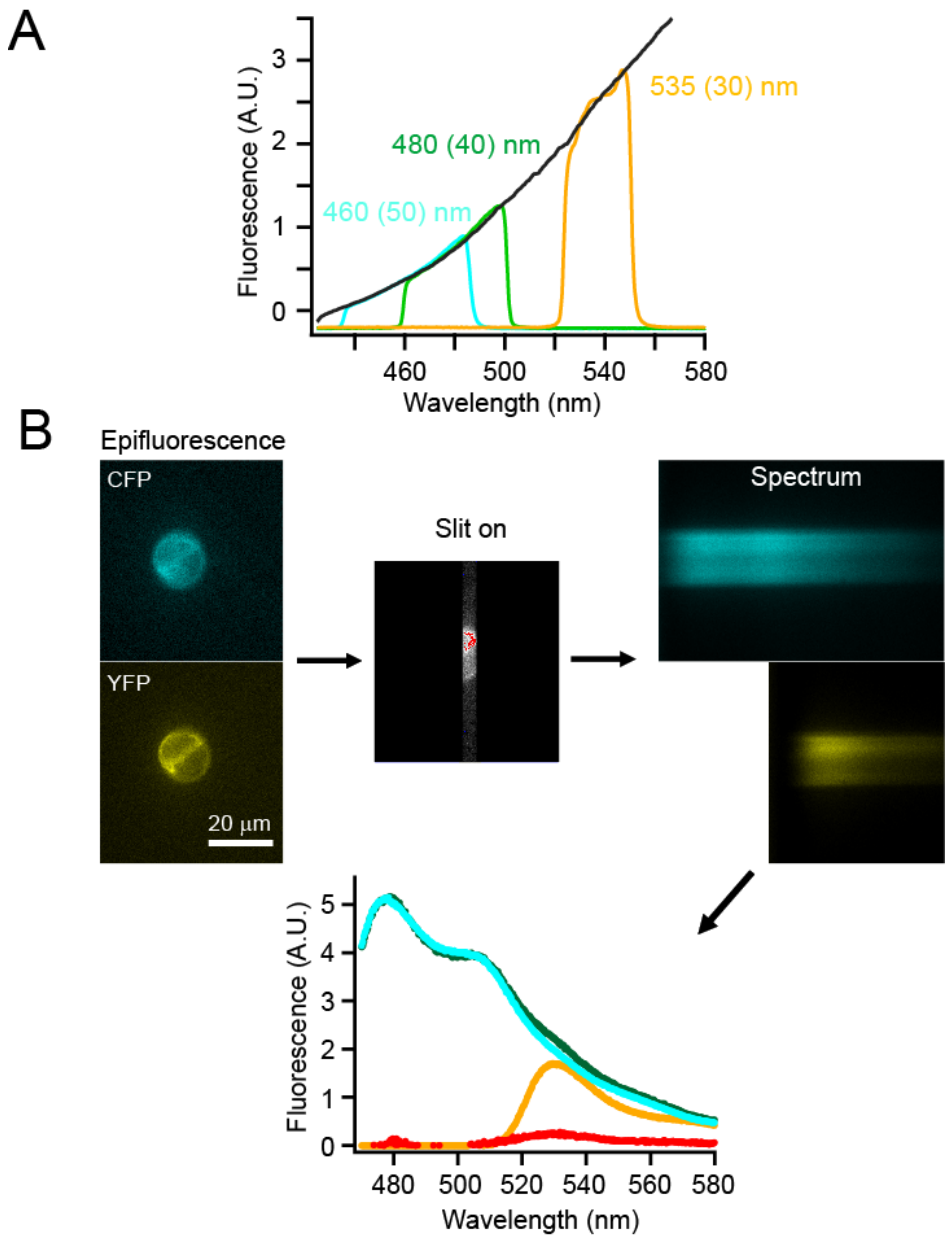
A
Fluorescence (A.U.)
0
1
2
3
460 (50) nm
480 (40) nm
535 (30) nm
460
500
540
580
Wavelength (nm)
B
Epifluorescence
CFP
YFP
20 μm
Slit on
Spectrum
Fluorescence (A.U.)
0
1
2
3
4
5
480
500
520
540
560
580
Wavelength (nm)

Figure S3

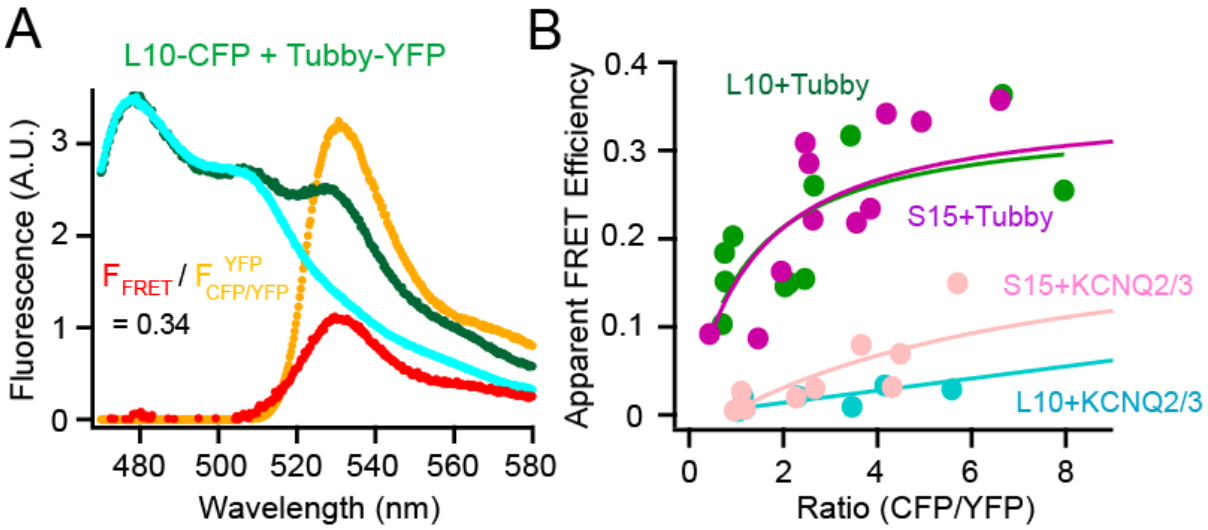
A
L10-CFP + Tubby-YFP
Fluorescence (A.U.)
3
2
1
0
F_{FRET} / $F^{YFP}_{CFP/YFP}$
= 0.34
480
500
520
540
560
580
Wavelength (nm)
B
Apparent FRET Efficiency
0.4
0.3
0.2
0.1
0
L10+Tubby
S15+Tubby
S15+KCNQ2/3
L10+KCNQ2/3
0
2
4
6
8
Ratio (CFP/YFP)